

Structural Characterization of Biocompatible Reverse Micelles using Small-Angle X-Ray Scattering, P Nuclear Magnetic Resonance and Fluorescence Spectroscopy

Emmanuel Odella, Ruben Dario Falcone, Marcelo Ceolin, Juana J. Silber, and N. Mariano Correa

J. Phys. Chem. B, **Just Accepted Manuscript** • DOI: 10.1021/acs.jpcb.7b11395 • Publication Date (Web): 28 Mar 2018

Downloaded from <http://pubs.acs.org> on March 28, 2018

Just Accepted

"Just Accepted" manuscripts have been peer-reviewed and accepted for publication. They are posted online prior to technical editing, formatting for publication and author proofing. The American Chemical Society provides "Just Accepted" as a service to the research community to expedite the dissemination of scientific material as soon as possible after acceptance. "Just Accepted" manuscripts appear in full in PDF format accompanied by an HTML abstract. "Just Accepted" manuscripts have been fully peer reviewed, but should not be considered the official version of record. They are citable by the Digital Object Identifier (DOI®). "Just Accepted" is an optional service offered to authors. Therefore, the "Just Accepted" Web site may not include all articles that will be published in the journal. After a manuscript is technically edited and formatted, it will be removed from the "Just Accepted" Web site and published as an ASAP article. Note that technical editing may introduce minor changes to the manuscript text and/or graphics which could affect content, and all legal disclaimers and ethical guidelines that apply to the journal pertain. ACS cannot be held responsible for errors or consequences arising from the use of information contained in these "Just Accepted" manuscripts.



***Structural Characterization of Biocompatible Reverse Micelles using
Small-Angle X-Ray Scattering, ^{31}P Nuclear Magnetic Resonance and
Fluorescence Spectroscopy***

Emmanuel Odella,^{*†a} R. Darío Falcone,[†] Marcelo Ceolín,[§] Juana J. Silber[†] and N.

Mariano Correa^{†*}

[†] *Departamento de Química. Universidad Nacional de Río Cuarto. Agencia Postal # 3.*

C.P. X5804BYA, Río Cuarto, Argentina.

[§] *Instituto de Investigaciones Fisicoquímicas Teóricas y Aplicadas. UNLP-CONICET*

(CCT-La Plata) Diagonal 113 y 64 (B1906ZAA), La Plata, Argentina.

^a *Current address: School of Molecular Sciences, Arizona State University, Tempe,*

Arizona 85287, United States.

[*] Dr. N. Mariano Correa, Dr. Emmanuel Odella Corresponding-Authors, E-mails:

mcorrea@exa.unrc.edu.ar; eodella@asu.edu

ABSTRACT: The most critical problem regarding the use of reverse micelles (RMs) in several fields is the toxicity of their partial components. In this sense, many efforts have been made to characterize non-toxic RMs formulations based on biological amphiphiles and/or different oils. In this contribution, the microstructure of biocompatible mixed RMs formulated by sodium 1,4-bis-2-ethylhexylsulfosuccinate (AOT) and tri-*n*-octylphosphine oxide (TOPO) surfactants dispersed in the *friendly solvent* methyl laurate was studied by using SAXS, ^{31}P NMR and, following the solvatochromic behavior of the molecular probe 4-aminophthalimide (4-AP). The results indicated the presence of RMs aggregates on TOPO incorporation with a droplet size reduction, and an increase on the interfacial fluidity in comparison with pure AOT RMs. When confined inside the mixed systems 4-AP showed red-edge excitation shift and confirms the increment of interfacial fluidity upon TOPO addition. Also, the partition between the external nonpolar solvent and the RMs interface, and an increase in both the local micropolarity and the capability to form hydrogen bond interaction between 4-AP and mixed interface were observed. The findings have been explained in terms of the nonionic surfactant structure and its complexing nature expressed at interfacial level. Notably, we show how two different approaches, i.e. SAXS and the solvatochromism of the probe 4-AP, can be used in a complementary way to enhance our understanding of the interfacial fluidity of RMs, parameter that is difficult to measure directly.

INTRODUCTION

The use and impact of reverse micelles (RMs) have been of growing interest during the past decade in both academic and technological applications. Properties such as their small size, thermodynamic stability, dynamic character, optical transparency and the peculiar interactions between the interface and the confined solvents are the key for chemical reactions,¹⁻³ enzymatic reactions⁴⁻⁸ and nanoparticle synthesis^{9,10} performed inside them. RMs are spatially ordered macromolecular assemblies of surfactants formed in nonpolar solvents, in which the polar head groups of the surfactants point inward toward a polar core and the hydrocarbon chains point outward toward the nonpolar medium.¹¹⁻¹³ The potential application of highly biocompatible aqueous RMs to food, cosmetic, and pharmaceutical industry as solubilization media of hydrophilic, hydrophobic, and amphiphilic functional materials displayed growing interest during the last years.¹⁴⁻¹⁸ Undoubtedly the most critical problem regarding a biocompatible use of RMs is the potential toxicity of their partial components. In these sense, many efforts have been made to characterize non-toxic RMs formulations based on biological amphiphiles and/or different oils. In particular, RMs systems dissolved in isopropyl myristate (IPM), ethyl myristate (EM), ethyl palmitate (EP) and ethyl oleate (EO) are quite promising.¹⁴⁻¹⁹ These long chain fatty acid esters are environmentally friendly with low toxicity and highly biodegradable, and most interestingly they show structural resemblance with the lipids in living systems.¹⁹⁻²²

On the other hand, it has been found that the addition of nonionic surfactants to the RMs interfaces formed by ionic surfactants, produces significant changes in water solubilization, droplet sizes as well as modifies the water or polar solvents structure inside the nanopool.^{20,23-25} Kundu et. al.^{20,21} explored the influence of nonionic surfactant Tween-85 on the properties of anionic sodium 1,4-bis-2-

ethylhexylsulfosuccinate (AOT) based micelle as well as RMs in fatty acid esters (EM, EP and EO). A comprehensive investigation of the micellization behavior at different mixed molar fraction of Tween-85 ($X_{\text{Tween-85}}$) was made by surface tension methods. Non-ideal mixing behaviors along with synergistic interaction between the constituent surfactants in the mixed micelles were evidenced. Also, mixed micelles illustrate favorable micellization behavior in terms of thermodynamic parameters, and fatty acid ester medium-based mixed RMs shows synergism in water solubilization capacity. Das et. al.⁶ studied the effect of replacing AOT by nonionic surfactant(s) of varying hydrophilic-lipophilic balance (HLB) on the structure, dynamics and activity of water encapsulated in RMs formed in IPM. Furthermore, they measured the enzymatic activity of α -chymotrypsin on the substrate Ala-Ala-Phe-7-amido-4-methyl coumarin and found that the enzymatic rate could either be enhanced or reduced depending on the HLB of the nonionic surfactant. Bardhan et. al.²⁶ studied the mixed cetyltrimethylammonium bromide and polyoxyethylene (23) lauryl ether microemulsions stabilized in 1-pentanol and IPM. The formation of mixed surfactant microemulsions was found to be spontaneous at all compositions, whereas it was endothermic at equimolar composition.

As summarized, there is clear evidence that the properties of RMs are modified when composed of mixed surfactants. However, to the best of our knowledge, all the studies are performed using nonionic surfactants which have a very long polar part in their moiety. Besides, most of those investigations are not focused on understanding one important parameter such as the fluidity of the interface. In view of the above, the present study aims at a precise characterization of the mixed systems formed by the AOT and the nonionic surfactant tri-*n*-octyl phosphine oxide (TOPO) dissolved in the friendly solvent methyl laurate (ML). In particular, TOPO has a very small polar head

(the P=O group) in comparison with its hydrophobic chains, and has more than one hydrocarbon tail and distinguishes from those that have only a single tail. Furthermore, the great versatility in the use of TOPO in different fields lies in the complexing properties of the P=O group.²⁷⁻³⁰

Previous studies performed in our group¹⁸ have shown very peculiar and interesting water properties inside AOT RMs formed in ML, and compared with the systems dispersed in IPM. The droplets size values, the maximum amount of water solubilized and the aggregation number (N_{agg}) of both AOT RMs are dissimilar considering the chemical structure of the external solvents and they can be explained taking into account the different non-polar solvent penetration to the interface. We have also characterized the mixed system formed with AOT and TOPO in *n*-heptane, and found interesting properties in both the micellar interface and the confined water behavior.^{27,30} We demonstrated both the existence of “bulk-like” water molecules at small W_0 values and the reduction of the mixed RMs size upon TOPO addition.

In this contribution we have investigated by different techniques such as small angle X-ray scattering (SAXS) and ^{31}P NMR spectroscopy, the size and morphology of the mixed RMs dispersed in ML, and the different molecular interactions between water and the mixed interface at W_0 ($W_0 = [\text{H}_2\text{O}]/([\text{AOT}] + [\text{TOPO}]) = 2$). In addition, we have introduced the molecular probe 4-aminophthalimide (4-AP) to explore the different environment properties. It is known that 4-AP is an excellent probe because its fluorescence lifetimes, spectra and quantum yields are affected greatly by its microenvironment.³¹⁻³³ We want to take advantages of the dependence of the emission band with the excitation wavelength in order to investigate complex systems like mixed RMs.

The results show that by increasing the molar fraction of TOPO ($X_{\text{TOPO}} = [\text{TOPO}] / ([\text{AOT}] + [\text{TOPO}])$), the water solubilization capacity diminished drastically. SAXS experiments show that mixed RMs at $W_0=2$ are formed spontaneously in every AOT:TOPO mixture investigated, and the droplet sizes decrease as the TOPO content increase. The data also suggest an increase on the droplets fluidity and the presence of the RMs aggregates at higher X_{TOPO} . The probe 4-AP undergoes a partition process between the external nonpolar solvent and the RMs interface and, this feature was used to obtain the “operational” critical micellar concentration (cmc_{op}) of every system investigated. Also, the solvatochromic study of 4-AP shows that the probe is capable of monitoring both an increase in the local micropolarity and, the capability to form hydrogen bond (H-bond) interaction between 4-AP and mixed interface when X_{TOPO} increases. Thus, we demonstrate the mixed RMs formation using the friendly ML solvent and, how the TOPO addition changes considerably the RMs properties, especially the interfacial fluidity. Under this perspective, the present mixed surfactants systems combine the unique characteristics of the water confined into AOT RMs and the complexity features of TOPO surfactant, in order to generate a special soft-template for nanoparticles synthesis, a venue that we are currently investigating.

EXPERIMENTAL SECTION

Materials: Sodium 1,4-bis (2-ethylhexyl) sulfosuccinate (AOT) and tri-*n*-octyl phosphine oxide (TOPO) were purchased from Sigma and were dried under vacuum prior use. Methyl Laurate (ML) from Sigma (HPLC quality), was used without purification and stored over molecular sieves (4 Å) before use. The molecular probe 4-aminophthalimide (4-AP) from Sigma was purified by repeated recrystallization from

ethanol.³¹ Doubly distilled water of conductivity less than $5 \mu\text{S cm}^{-1}$ was used in the experiments.

Methods: AOT and TOPO were individually dissolved in ML at a concentration of 0.25 M to prepare the respective stock solutions and then mixed in the desired proportions. The X_{TOPO} was varied from 0 to 1 in water solubilization capacity experiments and from 0 to 0.7 for both SAXS and spectroscopic experiments in the mixed systems. Aliquots of these stock solutions were used to make individual mixed RMs solutions with different water contents (W_0). Water was incorporated into each micellar solutions by using calibrated microsyringes. The solutions were agitated in a sonicating bath until the microemulsion was optically clear. A stock solution of 4-AP (1×10^{-3} M) was prepared in acetonitrile (Sintorgan, HPLC quality). The appropriate amount of this solution to achieve a final concentration of 1×10^{-4} M of the probe in the micellar medium was transferred into a volumetric flask, and the solvent was evaporated by bubbling dry N_2 ; then ML was added to the residue and the resulting solution was used to prepare the surfactants containing samples. To a cell containing 2 mL of 4-AP (1×10^{-4} M) in ML were added different amounts of surfactant and molecular probe stock solutions to obtain a given concentration of surfactant in the micelle media. Therefore, the absorption and emission of the probe were not affected by dilution. The lowest value for W_0 ($W_0=0$) corresponds to a system without the water addition.

General. SAXS experiments were performed at INIFTA (La Plata, Argentina, project “Nanopymes”, EuropeAid/132184/D/SUP/AR-Contract 331-896) facilities using a XEUS 1.0 equipment from XENOCSS with a $K\alpha$ -Cu radiation microsource ($\lambda=0.154$ nm). A PILATUS-100K detector was used with 543.4 mm sample to detector distance, which was calibrated using silver behenate. One-dimensional curves were

obtained by integration of the 2D data using the Foxtrot program (software developed on the SWING beamline).³⁴ The scattering intensity distributions as a function of the scattering vector (q) were obtained in the q range between 0.056 and 0.500 \AA^{-1} . The samples were placed in borosilicate glass capillary tubes of 1.5 mm of diameter and 10 μm of wall thickness. The scattering data were corrected for the background scattering from both the capillary tubes and the ML solvent. Data was analyzed using the indirect transformation procedure of Glatter.³⁵ The pair distance distribution function $\rho(r)$ was obtained by Fourier transform of the scattering intensity $I(q)$ as:

$$\rho(r) = \frac{1}{2\pi^2} \int_0^\infty q I(q) \sin(qr) dq \quad (1)$$

$$q = \frac{4\pi}{\lambda} \sin \frac{\theta}{2} \quad (2)$$

where q is the amplitude of the scattering vector, θ and λ are the scattering angle and the X-ray wavelength, respectively, and r is the distance in real space. The $\rho(r)$ function depends on the particle geometry and on the inner heterogeneity of the scattering density distribution in the particle, and their shape directly reflects the form of the RMs droplets.³⁶ The gyration radius (R_g) was calculated in two ways: (i) by using the Guinier plot (eq (4)) on the data sets in a defined small q range ($q \rightarrow 0$), we determined the value of R_g by using the Guinier's law:³⁵

$$I(q)_{q \rightarrow 0} = I_0 e^{-\left(\frac{q^2 R_g^2}{3}\right)} \quad (3)$$

$$\ln I(q)_{q \rightarrow 0} = \ln I_0 - \frac{q^2 R_g^2}{3} \quad (4)$$

(ii) by using the following equation:³⁶

$$R_{g,r}^2 = \frac{\int_0^{D_{\max}} \rho(r) r^2 dr}{2 \int_0^{D_{\max}} \rho(r) dr} \quad (5)$$

where D_{\max} is the maximum diameter of the particle, which is estimated from the $\rho(r)$ function satisfying the condition $\rho(r)=0$ for $r>D_{\max}$. In eq (5), $R_{g,r}$ means that the determination was in real space.

We have also performed ^{31}P NMR, steady state absorption and emission spectroscopy measurements. The instrumentation section is discussed in the supporting information (SI) in detail (section 2).

RESULTS AND DISCUSSIONS

1. Water Solubilization Capacity (W_0^{\max}). Water solubilization capacity (W_0^{\max}) of AOT:TOPO mixed systems (at $X_{\text{TOPO}}=0 \rightarrow 1.0$) in ML at 25.0 °C are presented in Figure 1. Single AOT system ($X_{\text{TOPO}}=0$) has been observed to solubilize a substantial amount of water, $W_0^{\max} \sim 43$ which is consistent with the literature reports.¹⁸ When the X_{TOPO} increases, the W_0^{\max} diminishes dramatically until $W_0^{\max} \sim 1$ for single TOPO/ML system.

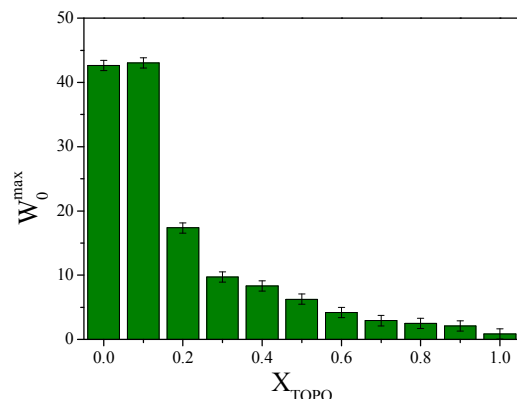
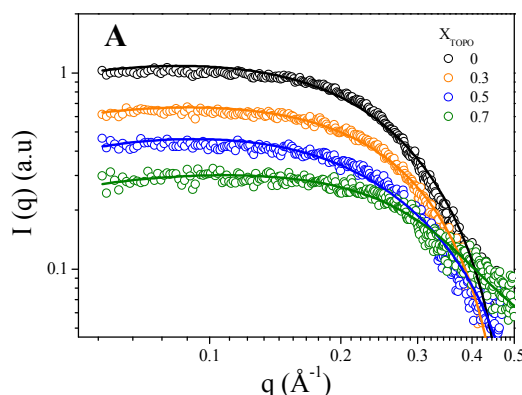


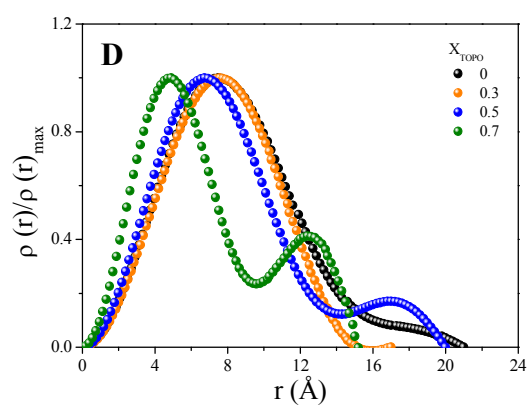
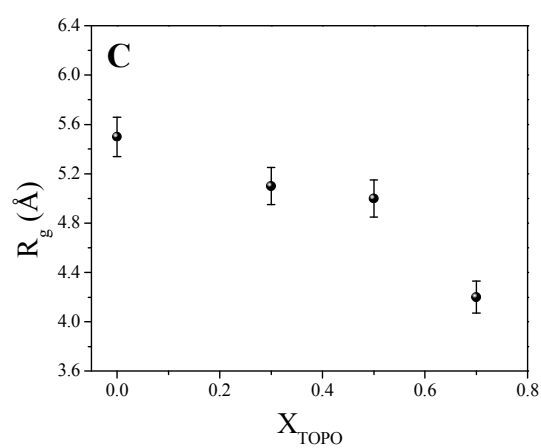
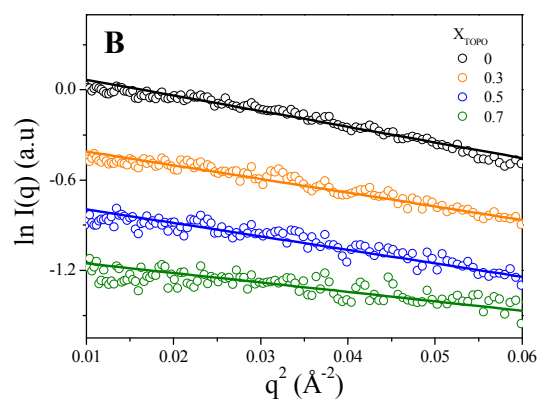
Figure 1. Maximum amount of water solubilized (W_0^{max}) in AOT:TOPO/ML mixed systems as a function of X_{TOPO} . $[\text{Surf.}]_{\text{T}}=0.1$ M.

The water solubilization capacities of RMs are determined by two phenomenological parameters such as the spontaneous curvature and the elasticity of the interfacial film, which are influenced by the constituents of the systems and the experimental conditions.^{37,38} In order to understand the factors that control the water solubilization capacity in these biocompatible systems, we performed SAXS experiments and we also take advantage of the solvatochromic behavior of a molecular probe sensible to different interfacial properties, results shown later in the work. A question may arise here that whether the water is effectively encapsulated by the surfactants creating a mixed RMs media at every X_{TOPO} investigated. In these sense, SAXS is a powerful technique for the direct structural investigations of the systems with the inner structuration falling in the colloidal domain.^{36,39}

2. Small Angle X-Ray Scattering (SAXS) Studies. SAXS measurements were carried out on the water/AOT:TOPO/ML systems at $W_0=2$ and different X_{TOPO} , where all the systems investigated exist in an isotropic single liquid phase. Figure 2 presents (A) the scattering functions, $I(q)$, (B) the Guinier plot ($\ln I(q)$ vs. q^2), (C) the radius of gyration (R_g) as a function of X_{TOPO} , (D) the resulting pair-distance

distribution functions, $\rho(r)$, and (E) the Kratky plot ($I(q) \cdot q^2$ vs. q). Here, we point out that since the chemical compositions of both the hydrocarbon oil and the hydrophobic part of the surfactants are similar, SAXS selectively detects the hydrophilic core of the RMs. Therefore, $\rho(r)$ must be recognized as a measure of the micellar core structure.^{36,40,41} The forward scattering intensity, $I(q \rightarrow 0)$, reaches $q=0$ parallel to q -axis for the water/AOT/ML and water/AOT:TOPO/ML systems, indicating the formation of spheroid type RMs.^{36,42} For water/AOT:TOPO/ML mixed systems, $I(q)$ in the small q region decrease with increasing X_{TOPO} , and in the high q region (or cross-section region) it shifts apparently toward the forward direction. These features of the scattering curves reflect a decrease in the micellar size with increasing the TOPO content. The R_g are shown in Figure 2C, and both R_g and those calculated from the $\rho(r)$ plot ($R_{g,r}$) are listed in Table S1 in the SI. Values of comparable magnitude were observed for Zhang et al.³⁶ for AOT RMs dissolved in analogous friendly oil like IPM at the same W_0 in presence of different alcohol types. As can be seen, Figure 2C and the values listed in Table S1 well reflect the size reduction with increasing TOPO content. The higher amount of TOPO at the interface layer produce smaller mixed RMs. Thus, AOT:TOPO/ML mixed system can solubilize less water than the AOT/ML RMs, and upon increasing the X_{TOPO} value the solubilization capacity of the mixed systems decrease (see Figure 1).





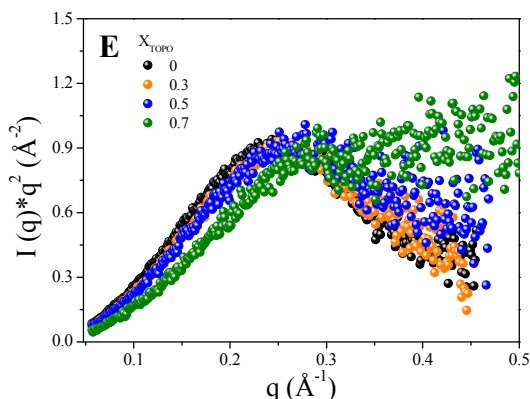


Figure 2. (A) Scattering intensities, $I(q)$, (B) the Guinier plot, (C) the radius of gyration (R_g) as a function of X_{TOPO} , (D) the corresponding normalized pair-distance distribution functions, $\rho(r)/\rho(r)_{\text{max}}$, deduced from the GIFT analysis and (E) the Kratky plot for water/AOT:TOPO/ML mixed RMs at $W_0=2$ and different X_{TOPO} . The solid lines in panel A represent GIFT fit.

The features in reciprocal space are well manifested in the real-space functions in a more intuitive way. In this sense, the $\rho(r)$ function is calculated according to eq (1) and showed in Figure 2D. For water/AOT/ML system, the curve presents a slightly asymmetric bell-shaped peak, suggesting that the RMs has a slightly elongated but nearly spherical shape.^{36,42} The peak apparently shifts to the lower r with increasing X_{TOPO} , indicating the decrease of the micellar size in mixed RMs, which is in good agreement with the results shown in Figure 2A, Figure 2C and Table S1. We can also verify that for higher TOPO content at the region near D_{max} , the distribution curve shows a behavior related to possible interactions between micellar structures that constitute the system, since the curve shows oscillations around this region.⁴³ In this sense, the bell-shaped peak profile accompanies a low hump or shoulders, particularly for $X_{\text{TOPO}} \geq 0.5$, mostly locate twice or thrice distance compared with the positions of the

first maximums in the $\rho(r)$ functions. The maximum peak in the $\rho(r)$ curve can be related to very small structures like discrete droplets, and the shoulder or the low hump peak to larger structures like oligomeric species such as dimers or trimmers due the strong interactions between RMs.^{36,44} Thus, this indicates that a large proportion of RMs are discrete droplets with a small proportion of oligomers in the system.

We use the Kratky plot (Figure 2E) to describe a qualitative approach of the structural characteristic such as interfacial fluidity.^{45,46} In the Kratky plot, the scattering curve for RMs with rigid interface exhibits a peak roughly shaped like a parabola. In contrast, RMs with fluid interfaces lack this characteristic peak and the curve profile increases monotonically in the large q region.^{45,46} In these sense, it can be deduced from Figure 2E that the interface of water/AOT/ML RMs is rigid, and the surfactant AOT forms a compact organized system in the biocompatible solvent. When X_{TOPO} content increases, the curve loses progressively its bell-shaped peak suggesting that the nonionic surfactant increases the mixed interfacial fluidity. The presence of the nonionic surfactant shields the AOT head group repulsion making the interface more fluid.^{20,47} The induced fluidity in turn increases the attractive interaction between the droplets, produces shape fluctuations, facilitates clustering of RMs and thereby limits the water solubilization capacity.⁶

3. Spectroscopic Studies of 4-AP

a. Absorption and Stationary Emission Studies of 4-A. Figure 3A shows the 4-AP absorption spectra by varying the surfactant concentration in the water/AOT/ML pure system at $W_0=2$. As it can be seen, the absorption spectra consist of two bands corresponding to different electronic transitions: (i) the band around 300 nm assigned to the $S_0 \rightarrow S_2$ ($\pi-\pi^*$ S_2 -LE) transition, named B_2 band, and (ii) the band around 350 nm assigned to the $S_0 \rightarrow S_1$ (S_1 -ICT) transition, that we will denote as B_1 band.³¹

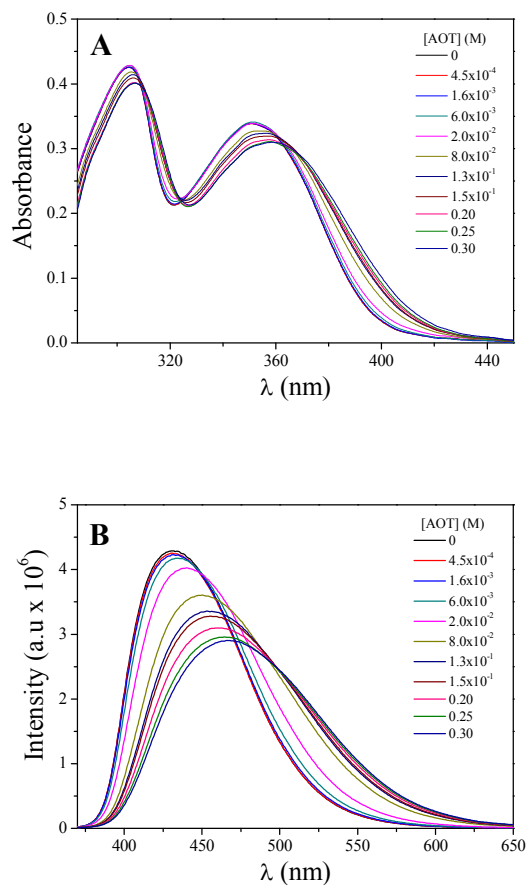


Figure 3. 4-AP absorption (A) and emission (B) spectra in water/AOT/ML pure RMs upon increasing the [AOT] at $W_0=2$. $\lambda_{\text{exc}}=350$ nm. $[4\text{-AP}]=1 \times 10^{-4}$ M.

In Figure 3A, it is observed also, a small bathochromic shift in the absorption maximum of both bands when the [AOT] increases, being the $\lambda_{\text{max}}B_1$ shift greater than for $\lambda_{\text{max}}B_2$. Furthermore, there is a slight change in the relative absorption intensity of both bands.

On the other hand, in the emission spectra shown in Figure 3B it can be seen that 4-AP shows a single emission band with maximum emission ($\lambda_{\text{emi}}^{\text{max}}$) at 434 nm in neat ML shifting bathochromically, toward $\lambda_{\text{emi}}^{\text{max}}=461$ nm, as the surfactant concentration increases. Also, an increase in bandwidth and a decrease in the emission intensity are

observed. Similar emission spectra were recorded for water/AOT:TOPO/ML mixed RMs for different X_{TOPO} at $W_0=0$ and 2 (see Figures S1 and S2, respectively). The decrease in the emission intensity is most likely due to an increase of the internal conversion rate as a consequence of the decrease in the separation between S_1 and S_0 after micellization. The enhancement on the H-bonding with the interfacial water may also be partly responsible for the reduction in fluorescence intensity.⁴⁸ Therefore, the emissive behavior indicates an increase in the interfacial micropolarity due to the polar head solvation. The effect of both the water confinement and the location of the probe can be observed in Figure S3 in the SI, which shows the absorption and the normalized emission spectra of 4-AP in both neat water and pure water/AOT/ML RMs at $W_0=2$. As can be seen, the $\lambda_{\text{emi}}^{\text{max}}$ of 4-AP is 89 nm blue-shifted compared to those in neat water ($\lambda_{\text{emi}}^{\text{max}}=550$ nm),⁴⁹ suggesting that the confined water in water/AOT/ML RMs is substantially less polar than neat water.⁴⁹

Figure S4 in the SI and Figure 4 show the $\lambda_{\text{emi}}^{\text{max}}$ values for 4-AP varying the $[\text{Surf.}]_T$ in water/AOT:TOPO/ML mixed systems at different X_{TOPO} and $W_0=0$ and $W_0=2$, respectively. A progressive red shift of $\lambda_{\text{emi}}^{\text{max}}$ with increasing $[\text{Surf.}]_T$ to ≈ 0.15 M was observed, remaining practically constant above this concentration. The profiles were all sigmoidal in nature and herein employed for critic micellar concentration (cmc) evaluation by fitting them with a Sigmoidal–Boltzmann equation (eq (6)):

$$A = \frac{a_i - a_f}{1 + e^{(x - x_0)/\Delta x}} + a_f \quad (6)$$

where the variable A corresponds to the $\lambda_{\text{emi}}^{\text{max}}$ value, the independent variable (x) is $[\text{Surf.}]_T$, a_i and a_f are the initial and final asymptotes of the sigmoid respectively, x_0 is the center of the sigmoid and Δx is the parameter which characterizes the steepness of

the function. The sigmoidal plot produces cmc value at x_0 ,⁵⁰ and the values for pure and mixed RMs at $W_0=0$ and 2 are listed in Table 1. It is customary to define this concentration value as “operational cmc” (cmc_{op}), since the cmc values depend on the method used to determine it.^{12,51}

As can be seen in Figure 4, the profiles present a smooth variation in the $\lambda_{\text{emi}}^{\text{max}}$ as a function of the $[\text{Surf.}]_{\text{T}}$. This behavior could reflect self-assembled systems that follow a sequential type association model.¹²

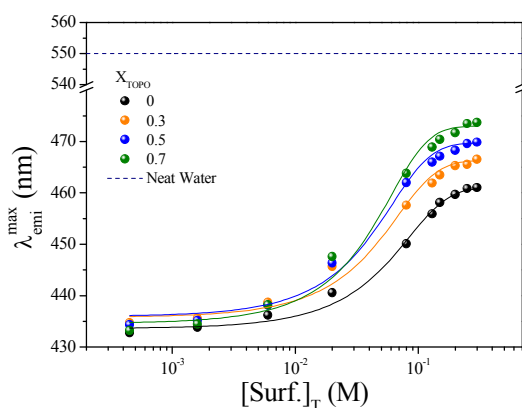


Figure 4. Variation of $\lambda_{\text{emi}}^{\text{max}}$ of 4-AP with $[\text{Surf.}]_{\text{T}}$ for water/AOT:TOPO/ML mixed RMs at $W_0=2$ and different X_{TOPO} . $\lambda_{\text{exc}}=350$ nm. The neat water value (---) is included for comparison.⁴⁹ The solid lines represent the sigmoidal fit using eq (6). $[4\text{-AP}]=1 \times 10^{-4}$ M.

The bathochromic shift exhibited in Figure 4 with increasing $[\text{Surf.}]_{\text{T}}$ indicates the change in micropolarity of the environment surrounding the probe molecule from the non-polar organic phase to a higher polarity microenvironment provided by the surfactants self-organization. Thus, based on the known behavior of this molecular probe,^{31,52,53} it can be deduced that the micropolarity of the microenvironment sensed by 4-AP increases in comparison to pure ML when the surfactant concentration increases. Indeed, 4-AP emits from two different micro-environments: the organic nonpolar

pseudophase and the pure or mixed RMs interfaces. Hence, it is possible to quantified the partition behavior of 4-AP taking into account the pseudophase model,^{12,54} by means of eq (7) (see calculation procedure of 4-AP partition constants in the SI, section 3 and 4). In this equation I_0 , $I_{\text{emi}}^{\lambda=430 \text{ nm}}$, ϕ_f , ϕ_b are the incident light, the fluorescence intensity at $\lambda_{\text{emi}}^{\text{max}}=430 \text{ nm}$ measured at the surfactant concentration considered, the fluorescent quantum yield of 4-AP in the organic solvent and bound to the RM interface (gathered in Table S2 of the SI), respectively. Figure 5 shows representative plots of the 4-AP emission intensity at $\lambda_{\text{emi}}^{\text{max}}=430 \text{ nm}$ as a function of $[\text{Surf.}]_T$ in the water/AOT:TOPO/ML mixed RMs at $W_0=2$ and different X_{TOPO} . The experimental data were fitted by eq (7) using a nonlinear regression method and the partition constants (K_p) values obtained are gathered in Table 1. The K_p values obtained in different mixed RMs at $W_0=0$ are also included.

$$I_{\text{emi}}^{\lambda=430 \text{ nm}} = \frac{I_0(\phi_f + \phi_b K_p [\text{Surf.}]_T)}{(1 + K_p [\text{Surf.}]_T)} \quad (7)$$

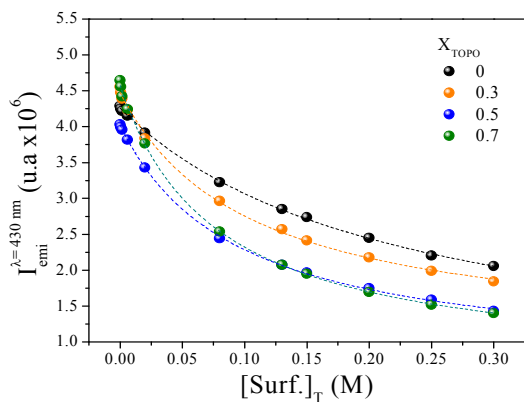


Figure 5. Representative plot of the 4-AP emission intensity at $\lambda_{em}=430$ nm as a function of $[\text{Surf.}]_T$ in the water/AOT:TOPO/ML mixed RMs at $W_0=2$ and at different X_{TOPO} . The data were fitted using eq (7). $[4\text{-AP}]=1\times 10^{-4}$ M.

Table 1. Operational Critical Micellar Concentration (cmc_{op}), Partition Constants (K_p), and REES ($\Delta\lambda_{emi}^{max}$) Values for 4-AP in Pure and Mixed Water/AOT:TOPO/ML Reverse Micelles at $W_0=0$ and 2

X_{TOPO}	cmc_{op} (mM)		K_p (M^{-1})		$\Delta\lambda_{emi}^{max}$ (nm)	
	$W_0=0$	$W_0=2$	$W_0=0$	$W_0=2$	$W_0=0$	$W_0=2$
0	16 ± 1	12 ± 2	4.6 ± 1.0	4.5 ± 0.3	17.4	14.0
0.3	15 ± 3	10 ± 2	8.6 ± 0.8	9.7 ± 0.9	11.6	8.7
0.5	13 ± 2	11 ± 1	11.4 ± 0.5	10.7 ± 0.4	8.4	5.8
0.7	12 ± 1	11 ± 2	12.0 ± 0.3	13.0 ± 0.8	7.6	2.6

It should be noted that the bathochromic shift is always observed when X_{TOPO} increases at fixed $[\text{Surf.}]_T$ (Figures S4 and 4). Also, this change is magnified once the aggregates are formed ($[\text{Surf.}]_T > \text{cmc}_{op}$). Then we can argue that the probe is capable of monitoring i) an increase in the local micropolarity and/or ii) an increase in the capability to form H-bond interaction between 4-AP and mixed interface. Although TOPO is a nonionic surfactant, the micropolarity sensed by 4-AP increase with TOPO incorporation which might suggest the existence of another factor that have influence on λ_{emi}^{max} . Durantini et. al.³¹ have made the Kamlet-Taft solvatochromic comparison method

(KTSCM) monitoring the frequencies corresponding to the B₁ absorption band and the emission frequencies corresponding to the emission maxima obtained exciting at $\lambda_{\text{max}}B_1$ and $\lambda_{\text{max}}B_2$. The KTSCM parameters obtained from the emission bands at the two monitored excitation wavelength show the same values, and the coefficients that measure the relative sensitivity of the frequencies to the polarity/polarizability (π^*) and H-bond acceptance (or electron pair donation ability to form a coordinated bond, β) are similar.³¹ This implies that 4-AP emission comes from a unique excited state which is affected in equal proportions for both the polarity and the H-bond acceptance or electron pair donation ability of the media. It is interesting to note that, 4-AP does not experiment any effect on its quantum yield when acts as hydrogen bond donor.³¹ Probably, the H-bond interaction of 4-AP is stronger with the TOPO polar head than AOT polar head at the interface. Consequently, this interaction could provide an additional stability of the S₁-ICT state and have influence on the different emission maxima observed. This behavior is supported from the well-known coordinating features of the phosphorous compound, considering the electronic properties of the trialkyl-substituted P=O group.^{27–30} The fact that there is a bathochromic shift of $\lambda_{\text{emi}}^{\text{max}}$ and a trend towards the value in neat water, would indicate a gradual weakening in the water-mixed interface interaction due TOPO addition. On the other hand, the K_p values increase when the X_{TOPO} increases (see Table 1). Interestingly, not significant changes were observed in K_p values by varying the water content. However, as mentioned above, there is a clear drop in the emission intensity when 4-AP is confined in the mixed RMs at W₀=2. The behavior could be only explained taking account the ϕ_b values of the probe at the two different W₀. As can be seen in the Table S2, the ϕ_b values at W₀=2 are almost 4 times lower than the ϕ_b values reported in the systems without water addition (W₀=0). This fact shows what is also already known for 4-AP:

the emission quantum yield decreases in solvents which are polar and protic and, much more in water.³¹ Also, from Table S2 it can be seen an independency on the ϕ_b values with the TOPO concentration, which shows that the quantum yield of the molecule is not affected by the hydrogen bond acceptor abilities of the surrounding.³¹ On the other hand, the weak water-mixed interface interaction due to the TOPO addition makes the water/AOT:TOPO/ML mixed RMs interface more fluid than the water/AOT/ML pure RMs, which favors the 4-AP partition toward the RMs pseudophase and explains the increase in K_p . Also, the H-bond interaction between 4-AP and TOPO seems to be a powerful driving force for the molecular probe to reach the mixed RMs interface.

b. Red-Edge Excitation Shift (REES) studies. A direct consequence of organized systems is the restriction imposed on the dynamics and mobility of their constituent structural units. Wavelength-selective fluorescence comprises a set of approaches based on the red edge effect in fluorescence spectroscopy, which can be used to directly monitor the environment and dynamics around a fluorophore in different complex system.^{55–57} A shift in the wavelength of maximum fluorescence emission toward higher wavelengths, caused by a shift in the excitation wavelength toward the red edge of absorption band, is known as red edge excitation shift (REES) phenomenon.^{57,58} This effect is mostly observed with polar fluorophores in motion restricted media such as very viscous solutions or condensed phases where the dipolar relaxation time of the solvent shell around a fluorophore is comparable to or longer than its fluorescence lifetime.⁵⁷ REES arises from slow rates of solvent relaxation (reorientation) around an excited state of the fluorophore, which is a function of the motional restriction imposed on the solvent molecules in the immediate vicinity of the fluorophore. Utilizing this approach, it becomes possible to probe the mobility

parameters of the environment itself (which is represented by the relaxing solvent molecules) using the fluorophore merely as a reporter group.⁵⁹

An example is shown in Figure S5 for the 4-AP emission spectra, exciting at $\lambda_{\text{exc}}=350$ nm and $\lambda_{\text{exc}}=400$ nm (the red edge of the band), in water/AOT/ML system at $W_0=0$. Identical experiments were made (data not shown) for all the systems studied. For 4-AP, the magnitude of REES ($\Delta\lambda_{\text{emi}}^{\text{max}}$) was defined as the difference in the emission maximum wavelength when exciting at $\lambda_{\text{exc}}=400$ nm and $\lambda_{\text{exc}}=350$ nm at $[\text{Surf.}]_T=0.1$ M: $\Delta\lambda_{\text{emi}}^{\text{max}}=(\lambda_{\text{emi}}^{\text{max}})_{\text{exc}=400 \text{ nm}}-(\lambda_{\text{emi}}^{\text{max}})_{\text{exc}=350 \text{ nm}}$. The Table 1 summarizes the REES values obtained. For AOT pure RMs in water absence ($W_0=0$), the $\Delta\lambda_{\text{emi}}^{\text{max}}=17.4$ nm found reflects the motion constrained environment that 4-AP senses at the interface. Similar results have previously been obtained for this probe in other RMs.⁵⁸ For mixed RMs (see Table 1), the decreases in the REES values with increasing X_{TOPO} , suggest that the interface become progressively more fluid with TOPO incorporation. Upon water addition, it can be seen that for both pure and mixed RMs, the $\Delta\lambda_{\text{emi}}^{\text{max}}$ values decreases suggesting that the dye's environment becomes significantly more fluid due the interface hydration. This phenomena is well known for many RMs^{31,58,59} and corroborates the formation of the systems in the friendly solvent. When comparing systems with the same water content ($W_0=2$), it can be seen that the TOPO incorporation decrease the REES magnitude. The decrease in the translation and rotation dynamics of water molecules interacting strongly with the AOT polar head is one of the causes for the REES effect manifestation.^{31,58,59} From this point of view, the presence of TOPO in the mixed interface would cause the progressive weakening in the water-mixed interface interaction and release of the hydration water, implying the gradual recovery of the polar solvent mobility and the lower REES values observed. This dehydration of the micellar interface is found to be essential for the size control of

micellar aggregates,⁶⁰ and the decrease in the REES effect due to the X_{TOPO} increase supports the RMs size modification (see Figure 2C), the changes observed in the Kratky representations (see Figure 2E) and the partition behavior of 4-AP (see Table 1).

4. ³¹P NMR Spectroscopy Studies. In order to gain more insight about the water-surfactants interactions and its impact on the counterions-surfactants interaction at the interface, we investigated the biocompatible mixed RMs using ³¹P NMR spectroscopy. Figure 6 shows ³¹P NMR spectra for pure TOPO/ML and AOT:TOPO/ML systems without and with water as described in Figure caption. The different peak positions of the P=O group of TOPO in homogeneous and micellar media are listed in Table 2. The P=O signal of TOPO/ML system is around $\delta=41.7$ ppm, and undergoes a downfield shift to $\delta=47.0$ ppm with the AOT incorporation (see Figure 6A and Table 2). This behavior is due to the large affinity of TOPO for Na^+ counterions at the interface; the strong interaction between P=O group and Na^+ causes a pronounced decrease in the electron density of the valence orbitals of phosphorus, explaining the downfield shift observed.^{27,30} By contrast, the situation is different when the surfactants are dissolved in polar solvents such as chloroform, where no formation of RMs is observed. Accordingly, the change in the δ is insignificant (see Table 2). Although chloroform is not polar enough, the δ for TOPO/ CDCl_3 and water/AOT:TOPO/ML are quite similar. As shown in our previous work, when the Kamlet-Taft solvatochromic comparison method was performed on the probe 4-AP, we use the following values for chloroform: polarity/polarizability parameter (π^*)=0.58, hydrogen bond acceptance or electron pair donation ability to form a coordinated bond (β)=0.1 and the hydrogen bond donation ability of the solvent (α)=0.44.^{31,61} Since π^* and α parameters have comparable values we believe that chloroform is capable to interact by H-bond interaction with the oxygen present in the TOPO polar head and could explain the similar δ observed for

both the system TOPO/ CDCl_3 -without self-organization- and mixed water/AOT:TOPO/ML. When water is incorporated in TOPO/ML system (Figure 6B), the P=O signal appears at $\delta=43.4$ ppm, 1.7 ppm downfield compared with the value observed in absence of water.

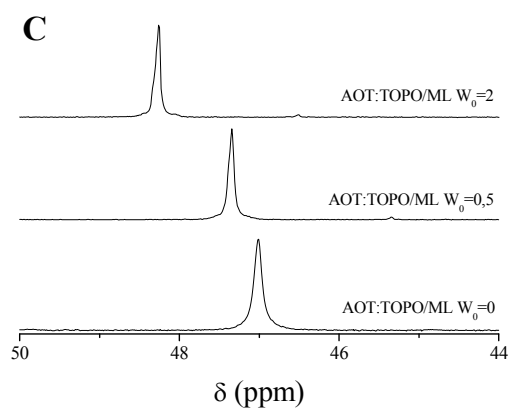
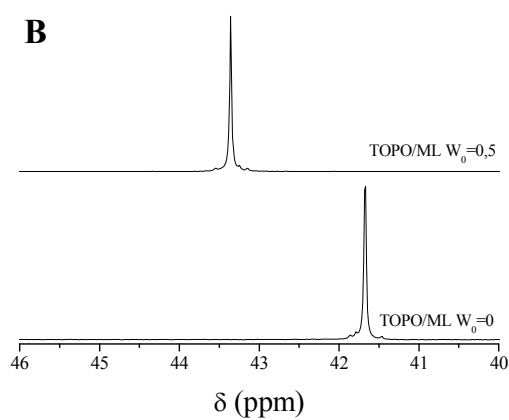
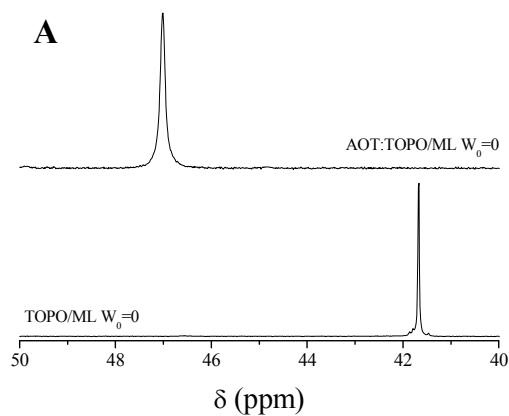


Figure 6. ^{31}P NMR spectra for (A) TOPO/ML pure and AOT:TOPO/ML ($X_{\text{TOPO}}=0.5$) mixed systems at $W_0=0$, (B) water/TOPO/ML pure system at different W_0 ($W_0=0$ and 0.5), and (C) water/AOT:TOPO/ML ($X_{\text{TOPO}}=0.5$) mixed systems at different W_0 ($W_0=0$, 0.5 and 2).

Table 2. ^{31}P NMR Chemical Shifts of P=O Group for TOPO in Homogeneous and Micellar Media

<i>Systems</i>	<i>X_{TOPO}</i>	<i>W₀</i>	<i>Chemical Shift (ppm)</i>
TOPO/ CDCl_3	1	0	47.9 ^a
AOT:TOPO/ CDCl_3	0.5	0	47.8 ^a
TOPO/ML	1	0	41.7
water/TOPO/ML	1	0.5	43.4
AOT:TOPO/ML	0.5	0	47.0
water/AOT:TOPO/ML	0.5	0.5	47.3
water/AOT:TOPO/ML	0.5	2	48.3

^a δ values obtained from ref. [27].

On the other hand, there is a slight downfield shift in the P=O signal upon increasing the W_0 in the mixed RMs (Figure 6C). At $W_0=0.5$, the P=O signal shift only 0.3 ppm downfield than the value at $W_0=0$ ($\delta=47.0$ ppm). Moreover, when water is encapsulated in small quantities into mixed RMs, the difference in the chemical shift is about 6 times less than the observed in the pure TOPO/ML system ($\Delta\delta=1.7$ ppm, see Table 2). This means that the water-mixed interface interactions are weaker than the water-pure AOT RMs interface interactions at very low W_0 values.

CONCLUSION

In the present study, we demonstrate the existence of pure AOT and mixed AOT:TOPO self-organized assemblies dispersed in non-toxic ML medium. When the X_{TOPO}

increases, the water solubilization capacity diminishes dramatically. SAXS curves reflect a decrease in the micellar size with increasing the TOPO content. Also, the analysis of the $\rho(r)$ function confirm the very small structures like discrete droplets with nearly spherical shape, slightly elongated, and shows larger structures like oligomeric species at higher TOPO content in the micellar solution. Furthermore, the nonionic surfactant increases notably the mixed interfacial fluidity. The overall behaviors were rationalized in terms of the great activity of the nonionic surfactant at the micellar interface and the increase of the effective packing parameter. On the other hand, the molecular probe 4-AP sense i) an increase in the local micropolarity and/or ii) an increase in the capability to form H-bond interaction between 4-AP and the mixed interface when TOPO is incorporated. Furthermore, the probe undergoes REES effect when is dissolved in the biocompatible RMs, and the decreases in the REES values with increasing X_{TOPO} confirm the increase of the interfacial fluidity by TOPO incorporation. It is important to note that the water-mixed interface interactions are weaker than the water-pure AOT interface interactions as suggested by the solvatochromic behavior of 4-AP and confirmed by ^{31}P NMR experiments.

We demonstrate that adding the nonionic TOPO surfactant into the AOT RMs produce remarkable changes at interfacial level, having control on the size, the interfacial fluidity and the water-mixed interface interactions, properties that were characterized in the work. In particular, both SAXS experiments and REES experienced by the probe 4-AP can be used together to understand the variations of the interfacial fluidity, property that become difficult to measure directly inside RMs.

Several properties of the mixed RMs studied here are similar to those previously reported for the surfactants mixture dissolved in n-heptane. However, those peculiar features take place in a biocompatible solvent such as ML, and the environmentally

friendly AOT:TOPO mixed RMs generated could be a promissory alternative in the green synthesis of nanoparticles using the RMs methodology.

Acknowledgments

Financial support from the Consejo Nacional de Investigaciones Científicas y Técnicas (PIP CONICET 112-201101-00204, PIP CONICET 112-2015-0100283), Universidad Nacional de Río Cuarto (PPI-UNRC 2016-2018), Agencia Nacional de Promoción Científica y Técnica (PICT 2012-0232, PICT 2015-0585 and PICT-2015-2151), and Ministerio de Ciencia y Tecnología, gobierno de la provincia de Córdoba (PID 2013) is gratefully acknowledged. E. O. is now a postdoctoral associate at Arizona State University. R. D. F., M. C., J. J. S. and N. M. C. are staff members of CONICET, Argentina.

SUPPORTING INFORMATION

Supporting Information Available; Section 1: Additional Figures and Tables from the main manuscript; Section 2: General procedure and instrumentation for ^{31}P NMR, steady state absorption and emission spectroscopy; Section 3: Calculation procedure of K_p ; Section 4: 4-AP fluorescence quantum yield determination in ML. This material is available free of charge via the Internet at <http://pubs.acs.org>.

REFERENCES

- (1) Bardhan, S.; Kundu, K.; Kar, B.; Chakraborty, G.; Ghosh, D.; Sarkar, D.; Das, S.; Senapati, S.; Saha, S. K.; Paul, B. K. Synergistic Interactions of Surfactant Blends in Aqueous Medium Are Reciprocated in Non-Polar Medium with Improved Efficacy as a Nanoreactor. *RSC Adv.* **2016**, *6*, 55104–55116.

- (2) Tang, L. L.; Ryabov, A. D.; Collins, T. J. Kinetic Evidence for Reactive Dimeric TAML Iron Species in the Catalytic Oxidation of NADH and a Dye by O₂ in AOT Reverse Micelles. *ACS Catal.* **2016**, *6*, 3713–3718.
- (3) Silva, O. F.; de Rossi, R. H.; Correa, N. M. The Hydrolysis of Phenyl Trifluoroacetate in AOT/n-Heptane RMs as a Sensor of the Encapsulated Water Structure. *RSC Adv.* **2015**, *5*, 34878–34884.
- (4) Moyano, F.; Falcone, R. D.; Mejuto, J. C.; Silber, J. J.; Correa, N. M. Cationic Reverse Micelles Create Water with Super Hydrogen-Bond-Donor Capacity for Enzymatic Catalysis: Hydrolysis of 2-Naphthyl Acetate by α -Chymotrypsin. *Chem. - A Eur. J.* **2010**, *16*, 8887–8893.
- (5) Shome, A.; Roy, S.; Das, P. K. Nonionic Surfactants: A Key to Enhance the Enzyme Activity at Cationic Reverse Micellar Interface. *Langmuir* **2007**, *23*, 4130–4136.
- (6) Das, A.; Parta, A.; Mitra, R. K. Modulation of Anionic Reverse Micellar Interface with Non-Ionic Surfactants Can Regulate Enzyme Activity within the Micellar Waterpool. *Colloid Polym. Sci.* **2016**, 1–12.
- (7) Moya-Ramírez, I.; García-Román, M.; Fernández-Arteaga, A. Waste Frying Oil Hydrolysis in a Reverse Micellar System. *ACS Sustain. Chem. Eng.* **2016**, *4*, 1025–1031.
- (8) Adlercreutz, P. Immobilisation and Application of Lipases in Organic Media. *Chem. Soc. Rev.* **2013**, *42*, 6406–6436.
- (9) Solanki, J. N.; Murthy, Z. V. P. Controlled Size Silver Nanoparticles Synthesis with Water-in-Oil Microemulsion Method: A Topical Review. *Ind. Eng. Chem. Res.* **2011**, *50*, 12311–12323.
- (10) Ganguli, A. K.; Ganguly, A.; Vaidya, S. Microemulsion-Based Synthesis of

- Nanocrystalline Materials. *Chem. Soc. Rev.* **2010**, *39*, 474–485.
- (11) Correa, N. M.; Silber, J. J.; Riter, R. E.; Levinger, N. E. Nonaqueous Polar Solvents in Reverse Micelle Systems. *Chem. Rev.* **2012**, *112*, 4569–4602.
- (12) Silber, J. J.; Biasutti, A.; Abuin, E.; Lissi, E. Interactions of Small Molecules with Reverse Micelles. *Adv. Colloid Interface Sci.* **1999**, *82*, 189–252.
- (13) Lépori, C. M. O.; Correa, N. M.; Silber, J. J.; Falcone, R. D. How the Cation 1-Butyl-3-Methylimidazolium Impacts the Interaction between the Entrapped Water and the Reverse Micelle Interface Created with an Ionic Liquid-like Surfactant. *Soft Matter* **2016**, *12*, 830–844.
- (14) Liu, D.-E.; Han, H.; Lu, H.; Wu, G.; Wang, Y.; Ma, J.; Gao, H. Synthesis of Amphiphilic Polyaspartamide Derivatives and Construction of Reverse Micelles. *RSC Adv.* **2014**, *4*, 37130–37137.
- (15) Rao, K. S.; Gehlot, P. S.; Trivedi, T. J.; Kumar, A. Self-Assembly of New Surface Active Ionic Liquids Based on Aerosol-OT in Aqueous Media. *J. Colloid Interface Sci.* **2014**, *428*, 267–275.
- (16) Chatzidaki, M. D.; Papavasileiou, K. D.; Papadopoulos, M. G.; Xenakis, A. Reverse Micelles As Antioxidant Carriers: An Experimental and Molecular Dynamics Study. *Langmuir* **2017**, *33*, 5077–5085.
- (17) Goswami, D.; Basu, J. K.; De, S. Lipase Applications in Oil Hydrolysis with a Case Study on Castor Oil: A Review. *Crit. Rev. Biotechnol.* **2013**, *33*, 81–96.
- (18) Girardi, V. R.; Silber, J. J.; Correa, N. M.; Falcone, R. D. The Use of Two Non-Toxic Lipophilic Oils to Generate Environmentally Friendly Anionic Reverse Micelles without Cosurfactant. Comparison with the Behavior Found for Traditional Organic Non-Polar Solvents. *Colloids Surfaces A Physicochem. Eng. Asp.* **2014**, *457*, 354–362.

- (19) Gupta, S.; Moulik, S. P. Biocompatible Microemulsions and Their Prospective Uses in Drug Delivery. *J. Pharm. Sci.* **2008**, *97*, 22–45.
- (20) Kundu, K.; Das, A.; Bardhan, S.; Chakraborty, G.; Ghosh, D.; Kar, B.; Saha, S. K.; Senapati, S.; Mitra, R. K.; Paul, B. K. The Mixing Behaviour of Anionic and Nonionic Surfactant Blends in Aqueous Environment Correlates in Fatty Acid Ester Medium. *Colloids Surfaces A Physicochem. Eng. Asp.* **2016**, *504*, 331–342.
- (21) Kundu, K.; Paul, B. K. Physicochemical Investigation of Biocompatible Mixed Surfactant Reverse Micelles: III. Aqueous NaCl Solubilization, Thermodynamic Parameters of Desolubilization Process and Conductometric Studies. *J. Surfactants Deterg.* **2013**, *16*, 865–879.
- (22) Boonme, P.; Krauel, K.; Graf, A.; Rades, T.; Junyaprasert, V. B. Characterization of Microemulsion Structures in the Pseudoternary Phase Diagram of Isopropyl palmitate/water/Brij 97:1-Butanol. *AAPS PharmSciTech* **2006**, *7*, E99–E104.
- (23) Bumajdad, A.; Eastoe, J.; Nave, S.; Steytler, D. C.; Heenan, R. K.; Grillo, I. Compositions of Mixed Surfactant Layers in Microemulsions Determined by Small-Angle Neutron Scattering. *Langmuir* **2003**, *19*, 2560–2567.
- (24) Li, Q.; Li, T.; Wu, J. Comparative Study on the Structure of Reverse Micelles. 2. FT-IR, ¹H NMR, and Electrical Conductance of H₂O/AOT/NaDEHP/n-Heptane Systems. *J. Phys. Chem. B* **2000**, *104*, 9011–9016.
- (25) Chatterjee, S.; Nandi, S.; Bhattacharya, S. C. Interface of AOT/Igepal CO720/cyclohexane/water Mixed Reverse Micelle by Spectroscopic Approach. *Colloids Surfaces A Physicochem. Eng. Asp.* **2006**, *279*, 58–63.
- (26) Bardhan, S.; Kundu, K.; Das, S.; Poddar, M.; Saha, S. K.; Paul, B. K. Formation, Thermodynamic Properties, Microstructures and Antimicrobial Activity of Mixed Cationic/non-Ionic Surfactant Microemulsions with Isopropyl Myristate as Oil. *J.*

- Colloid Interface Sci.* **2014**, *430*, 129–139.
- (27) Odella, E.; Falcone, R. D.; Silber, J. J.; Correa, N. M. Nanoscale Control Over Interfacial Properties in Mixed Reverse Micelles Formulated by Using Sodium 1,4-Bis-2-Ethylhexylsulfosuccinate and Tri-N-Octyl Phosphine Oxide Surfactants. *ChemPhysChem* **2016**, *17*, 2407–2414.
- (28) Pecheur, O.; Dourdain, S.; Guillaumont, D.; Rey, J.; Guilbaud, P.; Berthon, L.; Charbonnel, M. C.; Pellet-Rostaing, S.; Testard, F. Synergism in a HDEHP/TOPO Liquid–Liquid Extraction System: An Intrinsic Ligands Property? *J. Phys. Chem. B* **2016**, *120*, 2814–2823.
- (29) Rey, J.; Dourdain, S.; Berthon, L.; Jestin, J.; Pellet-Rostaing, S.; Zemb, T. Synergy in Extraction System Chemistry: Combining Configurational Entropy, Film Bending, and Perturbation of Complexation. *Langmuir* **2015**, *31*, 7006–7015.
- (30) Odella, E.; Falcone, R. D.; Silber, J. J.; Correa, N. M. How TOPO Affects the Interface of the Novel Mixed water/AOT:TOPO/n-Heptane Reverse Micelles: Dynamic Light Scattering and Fourier Transform Infrared Spectroscopy Studies. *Phys. Chem. Chem. Phys.* **2014**, *16*, 15457–15468.
- (31) Durantini, A. M.; Falcone, R. D.; Anunziata, J. D.; Silber, J. J.; Abuin, E. B.; Lissi, E. A.; Correa, N. M. An Interesting Case Where Water Behaves as a Unique Solvent. 4-Aminophthalimide Emission Profile to Monitor Aqueous Environment. *J. Phys. Chem. B* **2013**, *117*, 2160–2168.
- (32) Wetzler, D. E.; Chesta, C.; Fernández-Prini, R.; Aramendía, P. F. Dynamic Solvation of Aminophthalimides in Solvent Mixtures. *J. Phys. Chem. A* **2002**, *106*, 2390–2400.
- (33) Maciejewski, A.; Kubicki, J.; Dobek, K. The Origin of Time-Resolved Emission

- Spectra (TRES) Changes of 4-Aminophthalimide (4-AP) in SDS Micelles. The Role of the Hydrogen Bond between 4-AP and Water Present in Micelles. *J. Phys. Chem. B* **2003**, *107*, 13986–13999.
- (34) David, G.; Pérez, J. Combined Sampler Robot and High-Performance Liquid Chromatography: A Fully Automated System for Biological Small-Angle X-Ray Scattering Experiments at the Synchrotron SOLEIL SWING Beamline. *J. Appl. Crystallogr.* **2009**, *42*, 892–900.
- (35) Glatter, O. Small Angle Scattering and Light Scattering. In *Neutron, X-ray and light scattering*; Linder, P., Zemb, T., Eds.; Elsevier Science: New York, 1991; p 33–60.
- (36) Zhang, X.; Chen, Y.; Liu, J.; Zhao, C.; Zhang, H. Investigation on the Structure of Water/AOT/IPM/Alcohols Reverse Micelles by Conductivity, Dynamic Light Scattering, and Small Angle X-Ray Scattering. *J. Phys. Chem. B* **2012**, *116*, 3723–3734.
- (37) Leung, R.; Shah, D. O. Solubilization and Phase Equilibria of Water-in-Oil Microemulsions: II. Effects of Alcohols, Oils, and Salinity on Single-Chain Surfactant Systems. *J. Colloid Interface Sci.* **1987**, *120*, 330–344.
- (38) Leung, R.; Shah, D. O. Solubilization and Phase Equilibria of Water-in-Oil Microemulsions. *J. Colloid Interface Sci.* **1987**, *120*, 320–329.
- (39) Villa, C. C.; Moyano, F.; Ceolin, M.; Silber, J. J.; Falcone, R. D.; Correa, N. M. A Unique Ionic Liquid with Amphiphilic Properties That Can Form Reverse Micelles and Spontaneous Unilamellar Vesicles. *Chem. Eur. J.* **2012**, *18*, 15598–15601.
- (40) Shrestha, L. K.; Sato, T.; Aramaki, K. Intrinsic Parameters for Structural Variation of Reverse Micelles in Nonionic Surfactant (Glycerol α -

- Monolaurate)/oil Systems: A SAXS Study. *Phys. Chem. Chem. Phys.* **2009**, *11*, 4251.
- (41) Smith, G. N.; Brown, P.; James, C.; Kemp, R.; Khan, A. M.; Plivelic, T. S.; Rogers, S. E.; Eastoe, J. The Effects of Counterion Exchange on Charge Stabilization for Anionic Surfactants in Nonpolar Solvents. *J. Colloid Interface Sci.* **2016**, *465*, 316–322.
- (42) Shrestha, L. K.; Dulle, M.; Glatter, O.; Aramaki, K. Structure of Polyglycerol Oleic Acid Ester Nonionic Surfactant Reverse Micelles in Decane: Growth Control by Headgroup Size. *Langmuir* **2010**, *26*, 7015–7024.
- (43) Lucena, I. L.; Canuto, J. D. S.; Caroni, A. L. P. F.; Fonseca, J. L. C.; Neto, A. A. D.; Dantas, T. N. C. Characterization of Nonionic Surfactant Micellar Structures in Organic Solvents by Small Angle X-Ray Scattering (SAXS). *Colloids Surfaces A Physicochem. Eng. Asp.* **2012**, *408*, 48–56.
- (44) Hirai, M.; Kawai-Hirai, R.; Sanada, M.; Iwase, H.; Mitsuya, S. Characteristics of AOT Microemulsion Structure Depending on Apolar Solvents. *J. Phys. Chem. B* **1999**, *103*, 9658–9662.
- (45) Ichikawa, S.; Sugiura, S.; Nakajima, M.; Sano, Y.; Seki, M.; Furusaki, S. Formation of Biocompatible Reversed Micellar Systems Using Phospholipids. *Biochem. Eng. J.* **2000**, *6*, 193–199.
- (46) Putnam, C. D.; Hammel, M.; Hura, G. L.; Tainer, J. a. X-Ray Solution Scattering (SAXS) Combined with Crystallography and Computation: Defining Accurate Macromolecular Structures, Conformations and Assemblies in Solution. *Q. Rev. Biophys.* **2007**, *40*, 191–285.
- (47) Kundu, K.; Paul, B. K. Physicochemical Investigation of Biocompatible Mixed Surfactant Reverse Micelles: II. Dynamics of Conductance Percolation,

- Energetics of Droplet Clustering, Effect of Additives and Dynamic Light Scattering Studies. *J. Chem. Thermodyn.* **2013**, *63*, 148–163.
- (48) Saroja, G.; Samanta, A. Polarity of the Micelle-Water Interface as Seen by 4-Aminophthalimide, a Solvent Sensitive Fluorescence Probe. *Chem. Phys. Lett.* **1995**, *246*, 506–512.
- (49) Datta, A.; Mandal, D.; Pal, S. K.; Das, S.; Bhattacharyya, K. Solvation Dynamics in Organized Assemblies, 4-Aminophthalimide in Micelles. *J. Mol. Liq.* **1998**, *77*, 121–129.
- (50) Mondal, S.; Ghosh, S. Role of Curcumin on the Determination of the Critical Micellar Concentration by Absorbance, Fluorescence and Fluorescence Anisotropy Techniques. *J. Photochem. Photobiol. B Biol.* **2012**, *115*, 9–15.
- (51) De, T. K.; Maitra, A. Solution Behaviour of Aerosol OT in Non-Polar Solvents. *Adv. Colloid Interface Sci.* **1995**, *59*, 95–193.
- (52) Maciejewski, A.; Kubicki, J.; Dobek, K. Different Sources of 4-Aminophthalimide Solvation Dynamics Retardation inside Micellar Systems. *J. Colloid Interface Sci.* **2006**, *295*, 255–263.
- (53) Krystkowiak, E.; Dobek, K.; Maciejewski, A. Origin of the Strong Effect of Protic Solvents on the Emission Spectra, Quantum Yield of Fluorescence and Fluorescence Lifetime of 4-Aminophthalimide. *J. Photochem. Photobiol. A Chem.* **2006**, *184*, 250–264.
- (54) Lissi, E. A.; Engel, D. Incorporation of N-Alkanols in Reverse Micelles in the AOT/n-Heptane/water System. *Langmuir* **1992**, *8*, 452–455.
- (55) Sen, P.; Satoh, T.; Bhattacharyya, K.; Tominaga, K. Excitation Wavelength Dependence of Solvation Dynamics of Coumarin 480 in a Lipid Vesicle. *Chem. Phys. Lett.* **2005**, *411*, 339–344.

- (56) Satoh, T.; Okuno, H.; Tominaga, K.; Bhattacharyya, K. Excitation Wavelength Dependence of Solvation Dynamics in a Water Pool of a Reversed Micelle. *Chem. Lett.* **2004**, *33*, 1090–1091.
- (57) Chattopadhyay, A.; Mukherjee, S. Fluorophore Environments in Membrane-Bound Probes: A Red Edge Excitation Shift Study. *Biochemistry* **1993**, *32*, 3804–3811.
- (58) Durantini, A. M.; Darío Falcone, R.; Silber, J. J.; Mariano Correa, N. More Evidence on the Control of Reverse Micelles Sizes. Combination of Different Techniques as a Powerful Tool to Monitor AOT Reversed Micelles Properties. *J. Phys. Chem. B* **2013**, *117*, 3818–3828.
- (59) Chattopadhyay, A.; Mukherjee, S.; Raghuraman, H. Reverse Micellar Organization and Dynamics: A Wavelength-Selective Fluorescence Approach. *J. Phys. Chem. B* **2002**, *106*, 13002–13009.
- (60) Sethi, V.; Mishra, J.; Bhattacharyya, A.; Sen, D.; Ganguli, A. K. Hydrotrope Induced Structural Modifications in CTAB/butanol/water/isooctane Reverse Micellar Systems. *Phys. Chem. Chem. Phys.* **2017**, *19*, 22033–22048.
- (61) Kamlet, M. J.; Abboud, J. L. M.; Abraham, M. H.; Taft, R. W. Linear Solvation Energy Relationships. 23. A Comprehensive Collection of the Solvatochromic Parameters, ρ^* , α , and β , and Some Methods for Simplifying the Generalized Solvatochromic Equation. *J. Org. Chem.* **1983**, *48*, 2877–2887.

TOC GRAPHIC

